Subwavelength focusing with a multilayered Fabry-Perot structure at optical frequencies

Xuan Li,[1] Sailing He,[1,2,*] and Yi Jin[1,2]

[1]*Centre for Optical and Electromagnetic Research, Zhejiang University; JORCEP (Joint Research Center of Photonics of the Royal Institute of Technology (Sweden) and Zhejiang University), Zijingang campus, Hangzhou 310058, China*

[2]*Division of Electromagnetic Engineering, School of Electrical Engineering, Royal Institute of Technology, S-100 44, Stockholm, Sweden*

(Received 10 May 2006; revised manuscript received 27 October 2006; published 3 January 2007)

The Fabry-Perot resonance effect is studied in order to achieve subwavelength imaging at a far distance (e.g., about 10 wavelengths) from the source at optical frequencies. Two different structures (with matched and mismatched impedances) of alternative metal and air layers are considered first at a relatively short distance (e.g., about one wavelength) from the source. It is found that the impedance match is not necessary for subwavelength focusing since the Fabry-Perot resonance effect is utilized here. An appropriate period is chosen so that the Fabry-Perot resonance occurs in an evanescent regime, and consequently the evanescent waves near the Fabry-Perot resonance peak are amplified. With such a mechanism, a super lens with a resolution of about $\lambda_0/30$ (λ_0 is the wavelength in the air), acceptable sidelobes and a larger displacement range (when the thickness of the period is within such a displacement range, subwavelength focusing with acceptable sidelobes can be achieved) is designed. Subwavelength focusing (with a spotsize of $\lambda_0/12$) at a distance far away from the source is also realized in the presence of some material loss.

DOI: 10.1103/PhysRevB.75.045103 PACS number(s): 78.20.Ci, 42.30.Wb, 41.20.Jb, 78.45.+h

I. INTRODUCTION

The amplification of a broad spectrum of evanescent waves (produced by e.g., a point source) by a single layer of metal can lead to a subwavelength resolution, as noted first by Pendry[1] and later confirmed experimentally.[2] However, the thickness of this metal film has to be very small as compared with the wavelength. Thus it is impossible to transmit a subwavelength image to a far distance (e.g., the distance between the source and the image is more than $10\lambda_0$). In Ref. 2, the distance from the source to the image was only 75 nm (the wavelength is 365 nm). The diffraction effect has already degraded the imaging resolution at such a small distance (about $\lambda_0/5$) from the source (in such a small distance, a subwavelength resolution can also be achieved with the near-field scanning optical microscopy[3,4]) Therefore, a single layer of metal cannot transfer a subwavelength imaging to a far distance due to the material loss of the metal. In this paper we will study the subwavelength imaging in the area where the distance between the source and the image is larger than $10\lambda_0$.

Recently, Ramakrishna and Pendry[5,6] suggested a practical structure (as a superlens) to improve the subwavelength image in the near-field zone. They cut one metal slab into many thin layers and separated them (i.e., alternative metal and air layers). In such a structure, the metal and air layers have equal thickness but opposite signs of the real part of the permittivity (namely, −1 and +1). This structure is also less sensitive to the material loss. In structures of alternative metal and air layers, the relative permeability is always 1 (same as air), and thus the reflection is mainly determined by the effective refraction index (after homogenization), or equivalently, the effective impedance. In the present paper, an impedance match case refers to a situation when the effective (homogenized) refraction index (or effective impedance) of the multilayered structure is the same as that of air. Because of the impedance mismatch in Refs. 5 and 6, the total thickness of the structure must be much thinner than the wavelength (in order to reduce the reflection and the attenuation in the lossy metal). To reduce further the influence of the material loss on the subwavelength resolution, another type of structure with sandwiched metal layers has been proposed.[7] This structure is based on a different physical mechanism other than superlensing (the so-called canalization[8]). The canalization mechanism for subwavelength imaging at about one wavelength away from the source through a lossless multilayered structure was studied numerically in Ref. 7. The equal frequency contour (EFC) in the reciprocal lattice is flat, and this enables nearly all the spatial harmonics (including the evanescent components) of the source radiation to be transformed into propagating harmonics. These propagating harmonics have practically the same group velocity along the direction normal to the surface and nearly the same longitudinal components of the wave vector (see Ref. 7). The Fabry-Perot resonance condition can also be satisfied simultaneously for all the spatial harmonics and thus the transmission is enhanced. Inside such a structure, the field attenuation due to the material loss is uniform for nearly all the (propagating) spatial harmonics. At the output interface of the lens all the propagating harmonics are transformed back to the original spatial spectrum (including the evanescent components) as before entering the input interface of the lens. A good subwavelength image of a point source is thus achieved at the image plane (the distance from this plane to the back surface of the layered structure is equal to the distance between the source plane and the input surface of the layered structure). Their theoretical analysis is based on the theory of homogenization and transmission line at optical frequencies, for which the EFCs are completely flat. Choosing suitable permittivities and thicknesses for the metal and dielectric layers [see Eq. (2) below], one can obtain $\varepsilon_{\parallel}=1$ (i.e., impedance matched with air) and $\varepsilon_{\perp}=\infty$ from the homogenization theory. EFCs in such an anisotropic di-

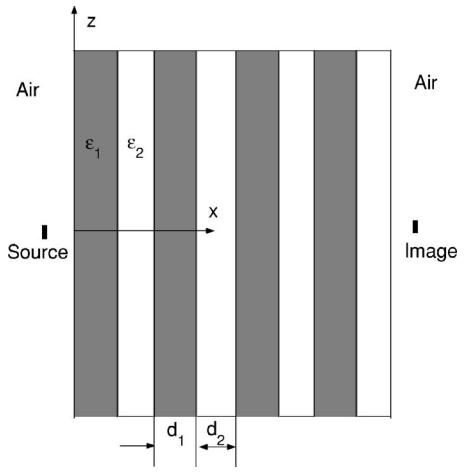

FIG. 1. Geometry of the periodic metal-dielectric structure studied in this paper. The period is $d=d_1+d_2$.

electric medium are planes parallel to the interfaces. In fact, EFCs for such a multilayered structure are not completely flat. The accuracy of the transmission line model for this multilayered structure is limited, and a more accurate model is needed for a more reliable analysis of the subwavelength imaging. In the present paper, we will analyze the dispersion relation and use a transfer matrix method to simulate the subwavelength imaging of a multilayered transmission device first at a relatively short distance (e.g., less than $2\lambda_0$) from the source. We found that the impedance match is not necessary for subwavelength imaging since the Fabry-Perot resonance effect is utilized here. Such a relaxation can leave us more space for the optimal design of a transmission device. To achieve a good subwavelength imaging at a far distance from the source with the material loss considered, we also relax the condition of impedance match and achieve a good resolution (i.e., spotsize of the focused image) of $\lambda_0/12$ in the present paper.

II. WORKING MECHANISM AND SUBWAVELENGTH IMAGING AT A SHORT DISTANCE

Figure 1 shows the schematic diagram for the multilayered structure studied in the present paper. In this structure, each period is composed of two thin layers whose thicknesses are d_1 and d_2 and permittivities are ε_1 (for dielectric) and ε_2 (for metal), respectively. For simplicity, we assume $\varepsilon_2=\varepsilon_2'+i\varepsilon_2''$ (complex) and $\varepsilon_1=\varepsilon_1'$ is real. Here we only consider the TM polarization (i.e., the magnetic field is perpendicular to the x-z plane). If each layer is very thin (compared with the wavelength), we can obtain the following effective (homogenized) anisotropic permittivity tensor (in the x and z directions) using the transmission line model in Ref. 7

$$[\varepsilon]=\begin{bmatrix}\varepsilon_\perp & 0\\ 0 & \varepsilon_\parallel\end{bmatrix}, \tag{1}$$

where $\varepsilon_\parallel=\frac{\varepsilon_1 d_1+\varepsilon_2 d_2}{d_1+d_2}$ and $\varepsilon_\perp=\left(\frac{\varepsilon_1^{-1}d_1+\varepsilon_2^{-1}d_2}{d_1+d_2}\right)^{-1}$. When the materials are lossless and condition $\varepsilon_1^{-1}d_1+\varepsilon_2^{-1}d_2=0$ is satisfied, one has $\varepsilon_\perp=\infty$ and each EFC (determined by the dispersion curve $k_x^2/\varepsilon_\parallel+k_z^2/\varepsilon_\perp=\omega^2/c^2$) is a straight (flat) line parallel to the z axis. However, in a lossy case we cannot apply the above effective medium theory. Otherwise, it will lead to some contradictory results. For example, condition $\varepsilon_1'^{-1}d_1+\varepsilon_2'^{-1}d_2=0$ will lead to

$$\varepsilon_\perp=\frac{(d_1+d_2)}{d_1}\left(\varepsilon'_1-i\frac{\varepsilon'_1\varepsilon'_2}{\varepsilon''_2}\right),$$

$$\varepsilon_\parallel=i\frac{\varepsilon''_2 d_2}{(d_1+d_2)}, \tag{2}$$

which gives $\varepsilon_\perp\to[(d_1+d_2)/d_1]\varepsilon_1'+i\infty$ when ε_2'' approaches 0 (lossless case). On the other hand, we know for a lossless case the effective permittivity (real valued) in the x direction is $\varepsilon_\perp=\infty$ (as we mentioned before), which is different from the limit of the lossy case. In fact, even for the lossless case the transmission line model is approximate and can only give a rough guidance for the analysis.

To make a more reliable analysis of the subwavelength imaging, we use an accurate model based on the following dispersion relation[9]

$$\cos(K_x d)=\cos(k_{1x}d_1)\cos(k_{2x}d_2)-\frac{1}{2}\left(\frac{k_{1,x}\varepsilon_2}{\varepsilon_1 k_{2,x}}+\frac{\varepsilon_1 k_{2,x}}{k_{1,x}\varepsilon_2}\right)\times\sin(k_{1x}d_1)\sin(k_{2x}d_2), \tag{3}$$

where $k_{1x}=\sqrt{\varepsilon_1 k_0^2-k_z^2}$, $k_{2x}=\sqrt{\varepsilon_2 k_0^2-k_z^2}$, $d=d_1+d_2$ and $k_0=2\pi/\lambda_0$ (we choose $\lambda_0=600$ nm in all our numerical examples). From the above equation, one sees that the Bloch wave number K_x is dependant on k_z [i.e., each EFC is determined by $K_x(k_z,d)$]. Figure 2 shows the EFCs in (k_z,K_x) plane for a lossless case for various sets of parameters (with

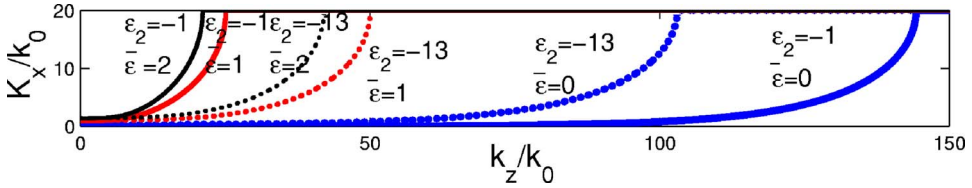

FIG. 2. (Color online) Equal frequency contours (lossless case) for $\lambda_0=600$ nm when condition $\varepsilon_1^{-1}d_1+\varepsilon_2^{-1}d_2=0$ is satisfied with period $d=15$ nm. The three solid curves are for $\varepsilon_2=-1$, and the three dotted curves are for $\varepsilon_2=-13$. The two longer blue (dark gray) curves are for $\bar{\varepsilon}\equiv(\varepsilon_1 d_1+\varepsilon_2 d_2)/(d_1+d_2)=0$, the two red curves (gray) are for $\bar{\varepsilon}=1$, and the two black curves are for $\bar{\varepsilon}=2$.

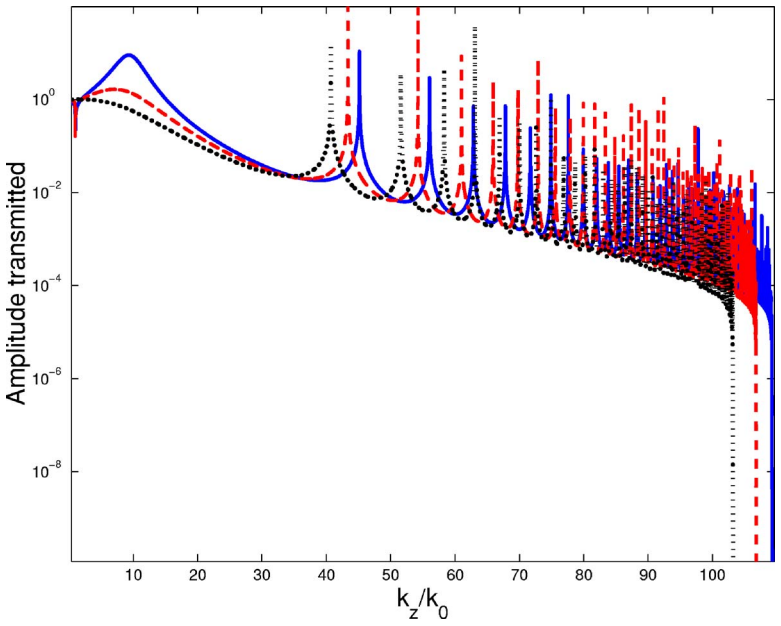

FIG. 3. (Color online) The transmission coefficient as a function of k_z/k_0 ($\bar{\varepsilon}=0$ and $\varepsilon_2=-13$). The dotted black curve is for $d=d_{\mathrm{FP}}=14.98$ nm (the corresponding resolution of the image is 40 nm); The red (gray) dashed curve is for $d=14.6$ nm (smaller than d_{FP}; the corresponding resolution of the image is 26 nm). The blue (dark gray) solid curve is for optimal $d=14.357$ nm (the corresponding resolution of the image is 18 nm, as indicated by the solid curve in Fig. 4 below).

$d=15$ nm) satisfying condition $\varepsilon_1'^{-1}d_1+\varepsilon_2'^{-1}d_2=0$ (this condition is always satisfied in the present paper). One sees from this figure that the EFCs can be very flat in a quite large range around $k_z=0$. Then we define $\bar{\varepsilon}=(\varepsilon_1'd_1+\varepsilon_2'd_2)/(d_1+d_2)$. Since condition $\varepsilon_1'^{-1}d_1+\varepsilon_2'^{-1}d_2=0$ is always satisfied in this paper, we have $\bar{\varepsilon}=\varepsilon'_1+\varepsilon'_2$. As $\bar{\varepsilon}$ decreases (from 2 to 1 and 0 in Fig. 2), the EFC (for the same $\varepsilon_2=-1$ or -13) becomes flatter around $k_z=0$ ($\bar{\varepsilon}=0$ gives the flattest EFC). Note that $\bar{\varepsilon}$ must be non-negative, otherwise some oscillations will appear in the EFCs around $k_z=0$. When $\bar{\varepsilon}$ is equal to 1 (the impedance match case considered in Ref. 7) or larger, the flat region of the EFC becomes wider as $|\varepsilon_2|$ increases from 1 to 13. The case of $\bar{\varepsilon}=0$ has an opposite trend, i.e., the flat region of the EFC becomes wider for smaller $|\varepsilon_2|$. From Fig. 2 one sees that the flat region of the EFC is the widest (the best for canalization) when $\bar{\varepsilon}=0$ (even its worst situation with large $|\varepsilon'_2|$ is still better than the best situation of $\bar{\varepsilon}=1$). Therefore, in the present paper we mainly study the case $\bar{\varepsilon}=0$ [e.g., when $\varepsilon_1=13$, $\varepsilon_2=-13$, $d=15$ nm, $d_1=d_2=7.5$ nm, we obtain $n_{\mathrm{eff}}=K_x(0,d)/k_0=0.2945$, which is mismatched to that of air] and compare with the corresponding performance for the case $\bar{\varepsilon}=1$. For example, when $\varepsilon_1=14$, $\varepsilon_2=-13$, and $d=15$ nm, condition $\bar{\varepsilon}=1$ gives $n_{\mathrm{eff}}=1.0486$ ($d_1=7.22$ nm, $d_2=7.78$ nm), which is quite close to 1 (the refractive index for air). Thus we can expect the reflection to be very small at the air-lens interface when $\bar{\varepsilon}=1$, and this is called an impedance match case in the present paper.

Inside the slab, all the propagating harmonics have almost the same K_x (longitudinal component of the wave vector) around $k_z=0$. To enhance the transmission through the slab lens (of finite thickness), we can choose N (the total number of the periods) to satisfy the following Fabry-Perot resonance condition

$$K_x(0,d)Nd=M\pi, \tag{4}$$

where M is an integer. We can scan d to obtain a function $F(d)$ which satisfies $K_x(0,d)N\cdot F(d)=M\pi$ (M is fixed during the scanning). Our numerical results (not shown here) have indicated that function $Y=F(d)$ is a monotonously decreasing function within the interval of [10 nm, c20 nm] and must have a cross point with the monotonously increasing function $Y=d$. The value of d at the cross point [i.e., $Y=F(d_{FP})=d_{\mathrm{FP}}$] would fulfill Fabry-Perot resonance condition (4). For example, for the case of $\bar{\varepsilon}=0$, if we choose $\varepsilon_1=13$, $\varepsilon_2=-13$, $d_1=d_2=d/2$, and $N=68$ (corresponding to a period around 15 nm), we can obtain $d_{\mathrm{FP}}=14.98$ nm (for $M=1$).

We use the transfer matrix method to compute the transmission coefficients for all the spatial harmonics (including the evanescent components) of the source radiation and obtain the image of the point source. We found that the spot size of the focusing can be improved further if the *actual period* d is a bit smaller than d_{FP}. This can be explained as follows. From the property of function $Y=F(d)$ it can be found that $K_x(0,d)Nd<M\pi$ when $d<d_{\mathrm{FP}}$. Since $K_x(k_z,d)$ increases from $K_x(k_z=0,d)$ as $|k_z|$ increases from 0 (see Fig. 2), some Bloch wave $K_x(k_z,d)$ with a nonzero $k_z=k_{FP}$ can satisfy the following Fabry-Perot resonance condition

$$K_x(k_{FP},d)Nd=M\pi. \tag{5}$$

From Fig. 3 one sees that as d decreases from $d=d_{\mathrm{FP}}$ the position of the Fabry-Perot resonance moves to a nonzero k_{FP} and every surface plasmon resonance peaks (many sharp peaks in the Fig. 3) also move along the same direction. If we choose a value of d less than d_{FP}, a broad Fabry-Perot resonance peak centered at a nonzero appears (the Fabry-Perot resonance is around $k_z/k_0=7.1$ on the red dashed curve in Fig. 3 for $d=14.6$ nm). From Fig. 3 one sees that the Fabry-Perot resonance peak for the case of $d=14.357$ nm (our optimal value for subwavelength focusing with acceptable sidelobes; corresponding to the blue solid line) is around $k_z/k_0=9.3$, which can be easily distinguished from the many sharp peaks caused by surface plasmon resonances. Larger k_z would lead to larger derivative $\partial K_x/\partial k_z$ (see Fig. 2) in the dispersion relation [Eq. (3)], and this makes the Fabry-Perot

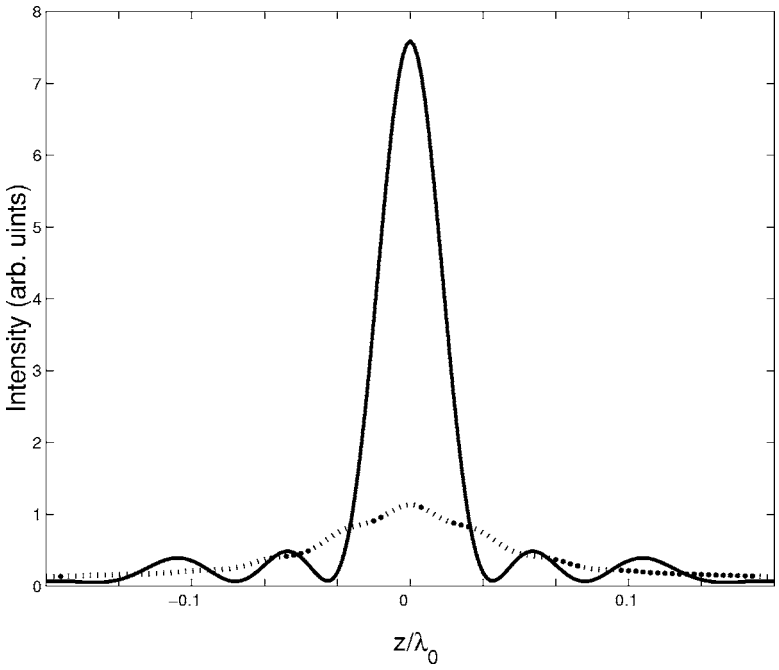

FIG. 4. The best-resolution images (of a point source) achieved by choosing optimal parameters for case $\bar{\varepsilon}=1$ (dotted line) and case $\bar{\varepsilon}=0$ (solid line).

effect concentrates on a smaller range of k_z around $k_z=k_{FP}$ (however the range of the Fabry-Perot resonance peak is limited, since the transmission coefficient of the propagating harmonics with $k_z<k_0$ cannot exceed 1). The evanescent components inside this range will be amplified, and thus the spotsize of the central peak in the image will become sharper. If d decreases further from 14.357 nm, the Fabry-Perot resonance would lead to larger sidelobes in the image of the point source, which will eventually distort the image. From the dispersion relation and Fig. 2 one can see that no Bloch waves in this multilayered structure can be excited by an incident evanescent wave with k_z larger than a certain value. Consequently, this part of incident evanescent waves cannot be transferred through the slab. This explains why there is a sudden and rapid decrease in the transmission function as $k_z>103k_0$ [for the dotted line with $d_{\mathrm{FP}}=14.98$ nm in Fig. 3; similar cut-off position in Fig. 2 for the dotted curve with $d=15$ nm (very close to $d_{\mathrm{FP}}=14.98$ nm)], $k_z>107k_0$ (for the dashed line in Fig. 3) or $k_z>109k_0$ (for the solid line also in Fig. 3) in Fig. 3. This k_z value is denoted by k_T (cut-off value). Larger k_T would allow more evanescent waves to be transferred through the slab, and thus lead to a better resolution. [Our numerical results have shown that the surface plasmon resonance peaks in Fig. 3 do not contribute to but degrade the resolution of the image.] Obviously, $d>d_{\mathrm{FP}}$ would lead to $K_x(0,d)Nd>M\pi$, and no value of k_z can satisfy the Fabry-Perot resonance condition. Thus, we should choose appropriate d (a bit smaller than d_{FP}) to obtain a good resolution while keeping the sidelobes low and acceptable according to the requirement of a specific application.

Note that in the present paper the amplification of evanescent components (see e.g., Fig. 3) is achieved by the Fabry-Perot resonance mechanism, but not the canalization mechanism (though the canalization mechanism plays an important role in transferring the evanescent components to an area far away from the source through the conversion between the evanescent components and the propagating components). If one chooses the impedance match case ($\bar{\varepsilon}=1$; as considered in Ref. 7) and $d=d_{\mathrm{FP}}$ in the impedance mismatch case, the Fabry-Perot resonance will occur at $k_z=0$ (corresponding to a propagating harmonics of the original spectrum of the image; the transmission coefficient for any original propagating harmonics is always less than 1) and thus this Fabry-Perot resonance cannot amplify any evanescent component. One of the unique ideas in the present paper is to choose d a bit less than d_{FP} so that the Fabry-Perot resonance occurs in an evanescent regime (i.e., $k_z>k_0$; the transmission coefficient for an evanescent wave can be much larger than 1; see Fig. 3), and consequently the evanescent waves near the Fabry-Perot resonance peak are amplified. Note that Fabry-Perot resonance is used in Refs. 7 and 8 merely for reducing the reflection at the air-lens interfaces and there is no amplification of any evanescent wave in Refs. 7 and 8. The amplification of evanescent components for the Fabry-Perot resonance mechanism is completely different from that for an LHM lens (which is based on the surface plasmon effect). To reduce the attenuation of the evanescent wave in the free space, we put the point source near the left air-lens interface. Thus the distance between the source and the image is less than to $2\lambda_0$ (i.e., imaging in an area close to the source) for this example.

Around d_{FP} there exists a displacement range $[d_{\min},d_{\max}]$, in which some subwavelength focusing with acceptable sidelobes can be achieved. A larger displacement range would indicate a better property for subwavelength focusing. The width of the displacement range for d can be extended to 0.9 nm in the case of $\bar{\varepsilon}=0$, whereas in the case of $\bar{\varepsilon}=1$ it is much smaller (e.g., 0.05 nm in a similar impedance-matched case considered in Ref. 7). For an impedance-matched case similar to the one considered in Ref. 7, the best resolution (defined as the half width of the central peak of the image) is about 50 nm according to our simulation results (the dotted curve in Fig. 4). However, in the case of $\bar{\varepsilon}=0$ (i.e., impedance match condition is relaxed) we can achieve a resolution

of about 18 nm (and an image of higher intensity; see the solid curve in Fig. 4) by choosing appropriate parameters.

Though the impedance is not matched between the lens and air when $\bar{\varepsilon}=0$, we can still see a large transmission, which is due to the Fabry-Perot resonance effect. Such a Fabry-Perot resonance effect enables us to obtain a better performance (in terms of the better resolution and larger displacement range) with this impedance-mismatched structure. From the above simulation results, it can be found that at the air-lens interface the impedance matching (i.e., same n_{eff} at both sides of the air-lens interface, as always satisfied in Ref. 7) is not necessary since the Fabry-Perot resonance mechanism is utilized here to enhance the transmission. Besides the Fabry-Perot mechanism, the reasons for us to choose this impedance-mismatched structure are as follows. (i) EFCs for case $\bar{\varepsilon}=0$ is flatter than EFCs for case $\bar{\varepsilon}=1$. Consequently, the Fabry-Perot condition holds approximately in a larger region of k_z around $k_z=0$. (ii) It is understandable that a multilayered structure with a smaller effective index n_{eff} (corresponding to a larger effective wavelength) has a larger displacement range, i.e., less sensitive to some small deviation of the layer positions (for the example in Fig. 2 we have $n_{\text{eff}}=0.29$ for $\bar{\varepsilon}=0$, whereas $n_{\text{eff}}\approx 1$ for $\bar{\varepsilon}=1$). Therefore, in the rest of the paper we will focus on this impedance mismatched structure (with $\bar{\varepsilon}=0$).

In the case of $\bar{\varepsilon}=0$ (mismatched impedance) and $d=13.96$ nm ($d_1=d_2=d/2$), the resolution and displacement range can be improved further if we use a smaller $|\varepsilon_2|$, e.g., $\varepsilon_1=6$, $\varepsilon_2=-6$ (obtained through e.g., some metal-dielectric composites[10]). The EFCs for $\varepsilon_1=6$ and $\varepsilon_2=-6$ is flatter [$K_x(0,d)$ is much smaller] than EFCs for $\varepsilon_1=13$ and $\varepsilon_2=-13$. The best resolution can be 14 nm, and the width of the displacement range to the thickness d can be larger than 1.25 nm.

Meanwhile we note that the total number of the plasmon resonance peaks increases with the total number of the layers, since each peak corresponds to the surface plasmon mode at a specific interface (see Ref. 5). When $\bar{\varepsilon}=0$, as $|\varepsilon_2|$ decreases, the EFCs become flatter and the structure could transfer more modes of evanescent waves to the other side of the slab, and consequently the resolution of the image may be improved. On the other hand, according to the dispersion relation, it can be shown that $K_x(0,d)$ becames smaller (as $|\varepsilon_2|$ decreases), and thus the total number N of the layers increases significantly (for a similar d) in order to satisfy Fabry-Perot resonance condition (4). However, when the total number of plasmon resonances becomes too large, large sidelobes appear in the image and the quality of the image becomes worse. Thus one should choose appropriate ε_2 according to the application and requirement. Obviously, the surface plasmon resonances degrade the quality of the image in the present mechanism of transmission device.

We have also used the FDTD (Ref. 11) simulation (commercial RSoft FullWAVE software) to verify the above subwavelength focusing for the impedance mismatch case (i.e., $\bar{\varepsilon}=0$). We choose $\varepsilon_1=13$, $\varepsilon_2=-13$, $d=14.41$ nm ($d_1=d_2=d/2$), $N=68$, and the distance between the point source and the left side of the lens is 20 nm. When we use the transfer matrix method the length L of the slab in z direction is infinite. However, in the FDTD simulation, we must set a finite value for L ($2\lambda_0$). The spotsize for the focused image in this FDTD simulation is about $\lambda_0/6$ (beating well the diffraction limit while the spotsize of the field distribution corresponding the point source at the left air-lens interface is over 60 nm), which is not as good as what the above transfer matrix method predicts. This is mainly due to the finite length (in the z direction) of the lens[12] and the attenuation of evanescent waves in free space.

III. SUBWAVELENGTH IMAGING AT A FAR DISTANCE WITH MATERIAL LOSS AND MISMATCHED IMPEDANCE

Based on the procedure described in the above section, we can obtain the following set of parameters as a numerical example for subwavelength imaging at a far distance from the source for the case of $\bar{\varepsilon}=0$ (i.e., impedance mismatch case): $\varepsilon_1=13$, $\varepsilon_2=-13$, $N=406$, and $d_{\text{FP}}=15.02$ nm (corresponding to $M=6$). We found that the optimal thickness is $d=14.84$ nm (i.e., $d_1=d_2=7.42$ nm). The image is quite far away (more than $10\lambda_0$) from the source. Figure 5 shows the corresponding subwavelength focusing results for several different material losses of the metal. The resolution of the image is 34 nm for the lossless case, and is 36 nm (about $\lambda_0/17$) when the imaginary part (representing the material loss) of the relative permittivity of the metal increases to 0.001. When $\varepsilon_2=-13+0.01i$, the half width of the focused spot increases to 50 nm ($\lambda_0/12$; still beat the diffraction limit even the intensity of the transmitted light is small due to the material loss). If we choose $\varepsilon_2=-13+0.4i$ with a much larger imaginary part (which is in the same order as the realistic value for silver), the half-width of the focused spot increases to 244 nm (a bit smaller than the half wavelength in free space). Therefore, the present multilayer Fabry-Perot structure can give sharp subwavelength focusing at 10 wavelength far away from the source, particularly when the material loss is small. Figure 6 gives the corresponding transmission coefficient functions of k_z under different levels of the small material loss of the metal.

From Fig. 6 one sees an obvious Fabry-Perot resonance peak (around $k_z/k_0=5$; as explained in the previous section when d is smaller than d_{FP}) when there is no material loss. Such a peak can improve the resolution of the subwavelength image. As the material loss of the metal increases, the transmission coefficient decreases (the decrement is larger for larger k_z under the same material loss). Furthermore, the decrement (caused by the loss) of the transmission coefficient at the surface plasmon resonance peaks is more significant.

Dispersion relation (3) is still valid when the material loss exists (e.g., a complex ε_2 represents the loss of the metal; ε_1 for the dielectric layers is kept real in our numerical example), and thus a complex Bloch vector function $K_x(k_z)$ can be numerically obtained.[13] Inside the multilayered structure, the direction of the group velocity of the wave is along the normal direction of EFCs, and the longitudinal (normal to the interface) component of the phase velocity is related to

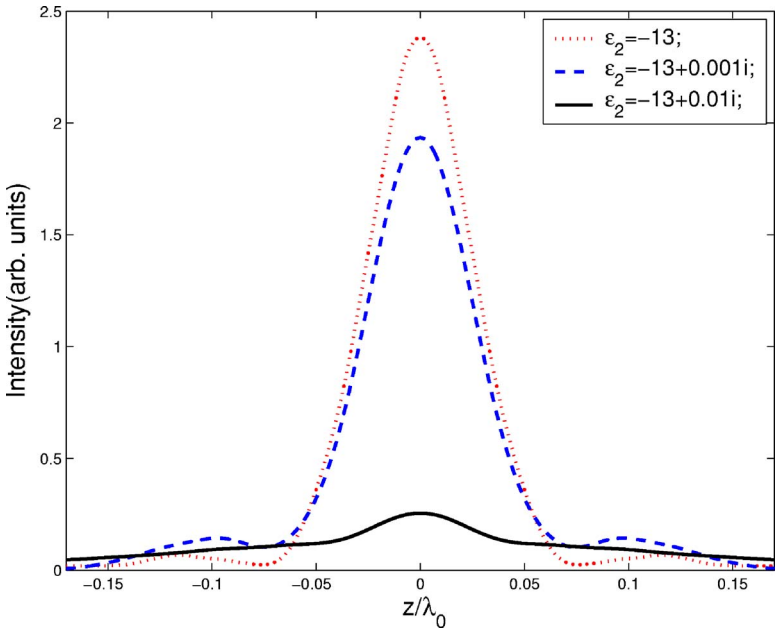

FIG. 5. (Color online) The influence of the material loss of the metal on the subwavelength imaging at a distance far away from the source.

$K_x(k_z)$. The imaginary part of the complex $K_x(k_z)$ has a physical meaning as the effective attenuation for such a wave (with k_z). The attenuation can be described by the following factor

$$L(k_z) = e^{-\mathrm{Im}(K_x(k_z))Nd}, \tag{8}$$

where $\mathrm{Im}[K_x(k_z)]$ is the imaginary part of $K_x(k_z)$. Figure 7 shows the attenuation factor $L(k_z)$ (which is 1 in lossless case). As k_z increases, the imaginary part of $K_x(k_z)$ increases and consequently the attenuation increases (see Fig. 7). This attenuation factor $L(k_z)$ will modulate the transmission spectra. This explains the rough range and decreasing shape of the transmission spectra shown in Fig. 6 (the shape of each curve in Fig. 7 is similar to that of the corresponding curve in Fig. 6).

IV. CONCLUSIONS

In the present paper we have studied the subwavelength focusing based on the Fabry-Perot resonance mechanism. The transfer matrix method has been used to analyze the multilayered transmission device consisting of alternative metal and air layers. We have found that the impedance match between the lens and air is not necessary for subwavelength focusing since the Fabry-Perot resonance effect is utilized here. The period d_{FP} of the multilayered structure satisfying the Fabry-Perot resonance condition (corresponding to the resonance peak around $k_z=0$) has been determined. We choose the period d a bit less than d_{FP} so that the Fabry-Perot resonance occurs in an evanescent regime (i.e., $k_z > k_0$), and consequently the evanescent waves near the Fabry-Perot resonance peak are amplified. With the help of such ampli-

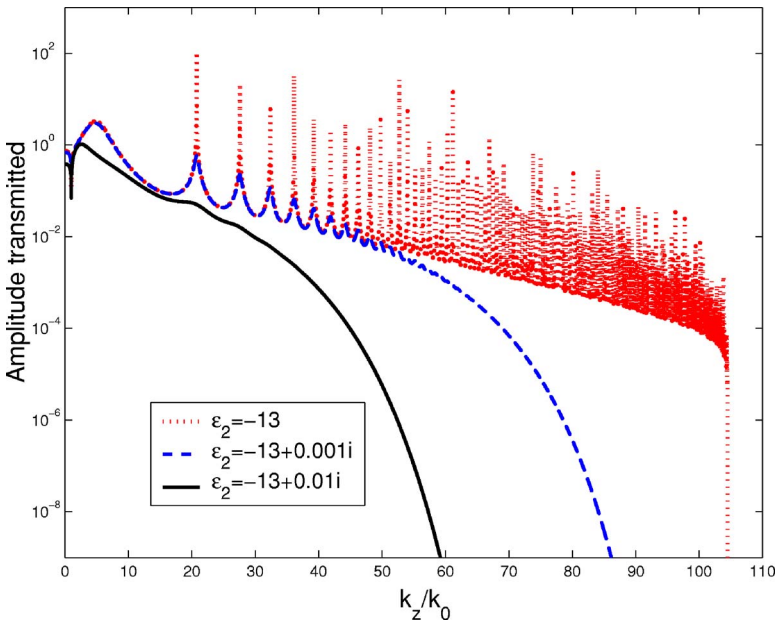

FIG. 6. (Color online) The transmission spectra corresponding to the subwavelength focusing in Fig. 5.

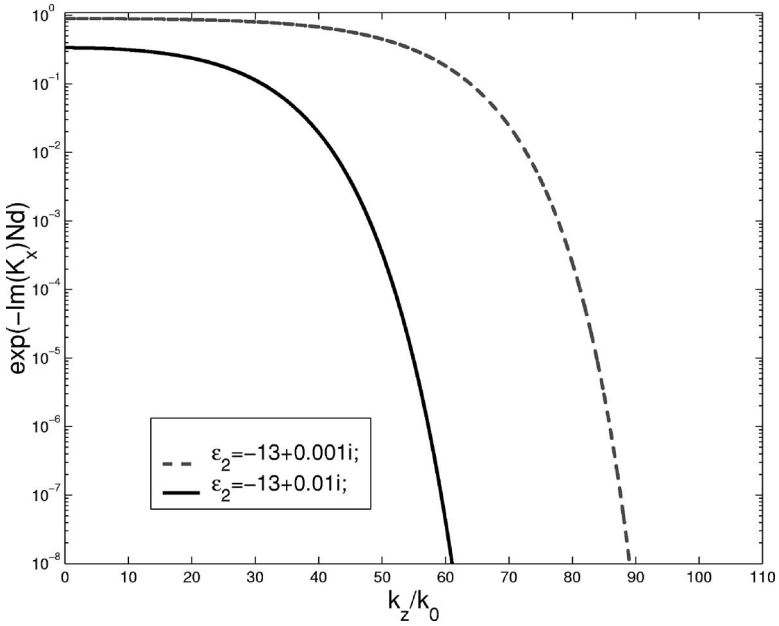

FIG. 7. The attenuation factor $L(k_z)$ caused by the material loss of the metal.

fication for the evanescent waves and the relaxation on the impedance, a good resolution (smaller than $\lambda_0/30$) with acceptable sidelobes at relatively short distance from the source (about $2\lambda_0$) is achived by choosing a suitable d (smaller than d_{FP}). Thus, the impedance mismatch case with $\bar{\varepsilon}=0$ would be more promising in achieving a better resolution with a larger displacement range. The influence of the material loss to the subwavelength imaging has been studied, and good subwavelength imaging at a distance far away from the source can still be realized in the presence of some material loss. In the present paper, the amplification of evanescent components is achieved by the Fabry-Perot resonance mechanism (completely different from the surface plasmon mechanism for an LHM superlens), but not the canalization mechanism. However, the canalization mechanism plays an important role in transferring the evanescent components to an area far away from the source through the conversion between the evanescent components and the propagating components.

ACKNOWLEDGMENTS

This work is partially supported by the National Basic Research Program (No. 2004CB719801) and an additional support from the Science and Technology Department of Zhejiang Province. We are also grateful to C. R. Simovski for helpful discussions.

*Email address: sailing@kth.se

[1] J. B. Pendry, Phys. Rev. Lett. **85**, 3966 (2000).
[2] N. Fang, H. Lee, C. Sun, and X. Zhang, Science **308**, 534 (2005).
[3] E. Betzig and R. J. Chichester, Science **262**, 1422 (1993).
[4] P. N. Prasad, *Nanophotonics*, 1st ed. (John Wiley & Sons, Hoboken, 2004), Chap. 3.
[5] S. A. Ramakrishna, J. Mod. Opt. **50**, 1419 (2003).
[6] J. B. Pendry and S. A. Ramakrishna, Physica B **338**, 329 (2003).
[7] P. A. Belov and Y. Hao, Phys. Rev. B **73**, 113110 (2006).
[8] P. Belov and C. R. Simovski, Phys. Rev. B **71**, 193105 (2005).
[9] L. Wu, S. He, and L. F. Shen, Phys. Rev. B **67**, 235103 (2003).
[10] W. S. Cai, D. A. Genov, and V. M. Shalaevl, Phys. Rev. B **72**, 193101 (2005).
[11] A. Taflove and S. C. Hagness, *Computational electrodynamics: The finite-difference time-domain method*, 2nd ed. (Artech House, London, 2000).
[12] L. Chen, S. He, and L. F. Shen, Phys. Rev. Lett. **92**, 107404 (2004).
[13] D. Soto-Puebla, M. Xiao, and F. Ramos-Mendieta, Phys. Lett. A **326**, 273 (2004).